Stockholm University

Bachelor Thesis

Degree Project in Geology 15 hp

Provenance of mafic outcrops and igneous clasts in Kobuk-Koyukuk sub-basin conglomerates and basin formation from sample geochemistry

Agata Kubiak

Stockholm 2017

Department of Geological Sciences
Stockholm University
SE-106 91 Stockholm
Sweden

Dedicated to C.E.K.

Provenance of mafic outcrops and igneous clasts in Kobuk-Koyukuk sub-basin conglomerates and basin formation from sample geochemistry

Abstract In western Alaska, huge basins occupy much of the landscape. There is some debate whether these basins are the remnant fore-arc of an accreted Jurassic-Cretaceous island-arc allochthon or a much younger formation related to continental rifting. The Yukon-Koyukuk basin contains as much an 8 km of sedimentary deposits which may hold the key to answering this question. To determine the tectonic setting of this basin, geochemical analyses of igneous clasts from the Kobuk-Koyukuk sub-basin sedimentary deposits as well as igneous rocks from an adjacent outcrop, are presented. The geochemistry of the igneous clasts preserve the distinctive Ta-Nb subduction signature while rocks from the outcrop have compositions equivalent to MORB ophiolite. Comparison to geochemistry from the Koyukuk Terrane indicates that the samples could be related by formation within the same island arc but likely at a different times and space. These results support the interpretation that the Koyukuk sub-basin is a fore-arc basin to the remnant Jurassic island arc.

1 Introduction

Kobuk-Koyukuk sub-basin (KKB) is one of several basins located within the Yukon-Koyukuk basin (YKB) (Fig. 1). Such basins are topographic depressions which often contain sediment deposited from adjacent highlands. A variety of tectonic processes can initiate the formation of a basin. Current studies present two possible tectonic processes responsible for the development of the KKB. One interpretation is that the basin represents a forearc of an ocean island-arc allochthon which collided with Laurentia in late Early Cretaceous time during the early stages of Brookian orogeny. The collision caused obduction of ocean ophiolite and island-arc onto the continent. Another interpretation suggests the basin is a later Paleogene feature caused by extension of the crust and subsequent sinking of the landscape. Until now the history and formation of the YKB has been interpreted by constraining the age, structure and provenance of bedrock in the bordering highland terranes and Koyukuk terrane (KT), and it has been assumed that that igneous clasts in the KKB sediment are from the eroded island-arc rocks of the KT. However, little work has been made to verify the hypothesis for the petrogenesis of these clasts (O´Brien et al., in press). These sediments may hold the key to understanding the formation of the basin and its relationship to bordering terranes (O´Brien et al., in press). This study investigates whether the tectonic provenance of igneous clasts from the KKB corresponds to the current interpretation correlating them to island-arc rocks, whether they represent a cogenetic suite of rocks, and if they are derived from KT rocks described by Box and Patton (1989). Previous work is limited and focuses on detrital Cr-spinel chemistry and isotopic composition and U-Pb ages of zircons (O'Brien et al., in press). This study is based on whole rock geochemical analysis of major and trace elements by X-Ray Fluorescence (XRF) and Laser Ablation Inductively Couples Mass Spectrometry (LA-ICP-MS) respectively. The analytical results are used to classify the rocks, determine whether the samples represent a cogenetic suite of rocks, and discriminate possible tectonic settings. This information will be used to discriminate between the hypotheses of a fore-arc basin versus a continental rift environment.

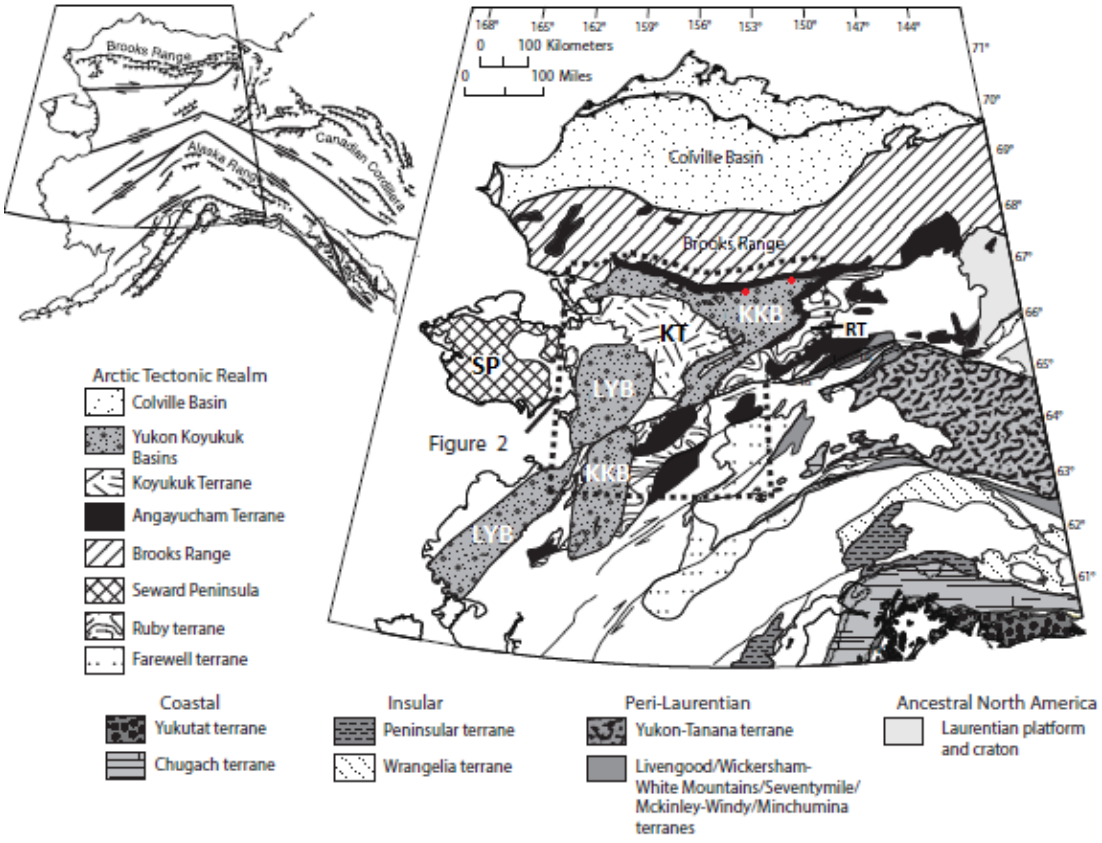

Figure 1. Regional geological map of the Yukon-Koyukuk province with bordering terranes. Red circles mark sample locations; western symbol locates samples collected in 2016 along the Alatna River (outcrop and igneous clasts), eastern symbol marks 2015 samples along the Koyukuk River (igneous clasts only) (map modified from O´Brien et al., in press). Sub-basins: KKB (Kobuk-Koyukuk basin), LYB (Lower Yukon Basin), RT (Ruby Terrane), KT (Koyukuk Terrane), SP (Seaward Peninsula).

2 Geological setting and history of the Yukon-Koyukuk basin

The Yukon-Koyukuk basin located in central-western Alaska covers c. 118,000 km^2 (O´Brien et al., in press). The province is interpreted to represent the remnant of an accreted Early Jurassic island-arc allochthon. The YKB basin forms a lowland which hosts the structurally elevated Koyukuk terrane. The KT is located between the limbs of the U-shaped Kobuk-Koyukuk sub-basin (KKB) and northeast of the Lower Yukon basin (LYB) (Fig. 1). The KKB is filed with clastic sediments, presumably the erosional debris from the surrounding terranes. The borderlands of YKB comprise Proterozoic and Palaeozoic continental rocks from the northern Brooks Range fold and thrust belt, the east Ruby Terrane intruded by calc-alkaline Tertiary volcanic rocks, and the west the flood basalts of the Seaward Peninsula. The Brooks Range orogen contains metamorphic assemblages from greenschist facies to high pressure/low temperature retrograded blueschist facies. A narrow band of mafic and ultramafic rock represent the Angayucham terrane, interpreted as a sequence of thrusted ophiolite; these rocks outcrop between the Brooks Range and the northern border of the KKB and dip southward under the province so that much of the unit is unexposed. The southernmost part of the YKB is dislocated dextrally 100-160 km to the west by the Tertiary Kaltag fault (Patton and Box, 1989). Reconstructions by Patton and Box (1989) reveal a very eventful history of island arc volcanism and accretion in Western Alaska. The rocks of YKB formed from off-shore arc volcanism which began in the Early Jurassic. The arc terrane began

approaching Laurentia and finally collided with the continent in the Early Cretaceous. The shortening of the crust and collision was a result of the early stages of Brookian orogenesis. In the initial stages, oceanic crust was subducted under the continent, subsequently the arc itself collided and was obducted onto the continent. During this collisional event arc-volcanism continued until the Albian. From isotopic dating the overthrusting of ocean crust is regarded as the cause of blueschist facies metamorphism in the Brooks Range. Later orogenic stages uplifted and eroded the arc, filling the KKB and LYB with Early to Late Cretaceous sediment. Deposits of sandstone and turbidites as much as 5-8 km deep contain clasts from volcanic, volcaniclastic and oceanic basalts, marine sediments and plutonic rocks. Today only a smaller fragment of the Jurassic island arc remain and this constitutes the KT highland of the YKB.

3 Field relations and Sampling

KKB sedimentary deposits have been divided into two stratigraphic units. A lower unit which is exposed over most the basin and an upper unit exposed at the edges of the basin where it meets the bordering terranes of the Books Range and the Ruby Terrane. The upper unit is described by Patton and Box (1989) as 2500 m of deltaic polymict debris from the borderlands. They further describe the upper unit as fluvial and shallow marine conglomerate, sandstone and shale. The lower unit is depicted as a 6500m deep section of channels and lobes of turbidite mudstone and greywacke rich in volcanic lithic fragments from the Angayucham terrane, KT and minor occurrences of metamorphic rocks. All samples were collected by V. Pease. Samples beginning VP15 and samples VP16-23 (a,c,d,e) consist of igneous lithic fragments imbedded in conglomerate. Samples VP16-22 (a,b,c) represent samples of pillow basalt and gabbro from an ophiolite outcrop (cover image). Sample photographs are displayed in appendix I. All samples were collected along the Alatna and Koyukuk rivers as indicated in figure 1. Rocks with the least weathering, fractures, veins and alterations were selected as samples. Samples collected in 2016 are from the Alatna river and are labelled VP16 and samples collected in 2015 along the Koyukuk river are labelled VP15. The samples are cobbles ranging from aphanitic to fine-medium grained. The size of the samples was chosen to represent an average rock composition in the subsequent sample preparation and analysis.

4 Methods

Samples were crushed using a Retsch RS200 swing mill at 1400 rpm between 120-50 sec. Aliquots of rock powder mixed with Lithium borate flux ($66\%Li_2B_4O_7+34\%LiBO_2$) in proportions of 2:5 were fused into homogenous glass discs using a Phoenix VDF autofuser. All analyses were conducted at the Department of Geological Sciences, Stockholm University. Major element analysis was performed by XRF using a Rigaku ZSX Primus II. Twenty-four international standards were used for instrument calibration. Standards AGV2, BRC2 and RGM1 were used as internal standards and run every 10^{th} sample to confirm instrument performance. Major elements are presented in weight percent (wt %) oxides (Table 1). Trace elements were measured via LA-ICP-MS on fragments of the same glass discs used for XRF. The fragments were mounted in epoxy and polished prior to analysis. LA-ICP-MS analysis was performed using a 193 Excimer laser combined with a ThermoFisher X-series II quadrupole mass spectrometer following standard procedures. The instrument was tuned using international standard NIST-612; secondary standards BCR-2 and SARM-1 and an internal Si standard were used to confirm instrument performance. Results are reported in parts per million (ppm) (Table 1). P and Cs were below detection limits and are not reported in the dataset. The detailed analytical procedure and method description is provided in the appendix (II).

Table 1. Geochemical analyses of clasts and igneous samples from the KKB.

	VP15-10	VP15-11	VP15-12	VP15-13	VP16-22a	VP16-22b	VP16-22c	VP16-23a	VP16-23c	VP16-23d	VP16-23e
					Major elements, Anhydrous wt%						
SiO_2	49.2	47.1	50.2	51.5	49.0	45.9	48.7	51.9	63.1	50.8	52.8
Al_2O_3	14.83	18.23	16.55	15.80	14.89	15.69	16.21	17.13	16.00	16.58	18.91
CaO	11.13	16.33	8.19	8.66	10.00	10.84	12.02	7.95	3.20	7.43	9.04
MgO	6.41	6.84	3.76	5.74	6.98	8.00	9.38	6.22	3.08	6.09	2.79
MnO	0.23	0.18	0.20	0.23	0.19	0.22	0.20	0.24	0.17	0.25	0.15
P_2O_5											
Fe_2O_3	1.90	1.28	2.17	1.81	1.85	2.05	1.50	1.67	1.98	1.90	2.30
FeO	9.49	6.39	10.83	9.05	9.24	10.24	7.48	8.35	3.96	9.49	6.58
Na_2O	2.9	1.9	4.0	4.1	4.1	3.6	2.9	3.5	4.6	4.1	3.6
K_2O	0.76	0.12	0.64	0.41	0.06	0.04	0.04	0.48	2.69	0.63	1.94
TiO_2	1.99	0.92	2.15	1.62	2.54	2.19	0.74	1.47	0.60	1.62	0.94
					Volatiles, wt%						
LOI	2.33	3.88	3.03	2.50	3.74	5.81	3.66	3.99	3.63	4.76	6.83
					Trace elements, ppm						
Y	31	16.1	32	31	26.6	21.7	16.2	23.9	19.5	23.3	20.5
Sm	5	2	4	4	4	5	2	3	4	3	5
Pr	3.6	0.95	2.8	2.5	3.0	3.3	0.66	1.99	3.5	2.1	4.4
Tb	0.89	0.42	0.83	0.79	0.77	0.72	0.42	0.71	0.54	0.74	0.66
Dy	5.8	2.9	5.7	5.5	5.0	4.4	3.0	4.9	3.4	4.9	4.0
Nd	17.1	5.2	14.0	13.2	14.8	15.9	3.9	10.5	15.8	11.0	20
Th	1.17	0.11	0.67	0.64	0.81	1.11	0.09	0.46	2.1	0.33	1.9
Sr	610	280	410	168	246	130	37	293	240	360	440
Ni	40	39	15.9	29	53	194	119	56	9.0	41	24
Ce	24.4	5.2	17.7	16.1	19.5	21.7	3.7	12.8	23.9	12.7	29
Zr	141	37	107	95	107	116	32	103	109	82	94
Sc	43	40	31.7	40	41	39	47	40	14.8	46	32
La	10.3	1.9	7.3	6.6	8.3	9.4	1.24	5.1	10.8	5.1	13.4
Eu	1.87	1.16	1.66	1.48	1.69	1.69	0.69	1.36	1.18	1.32	1.35
Tm	0.49	0.26	0.52	0.49	0.41	0.30	0.29	0.42	0.31	0.42	0.30
U	0.36	0.07	0.33	0.32	0.28	0.26	0.03	0.21	1.28	0.16	0.72
Ba	132	31	570	340	450	153	65	267	430	330	340
Lu	0.44	0.25	0.51	0.47	0.38	0.29	0.29	0.44	0.35	0.43	0.33
Ta	0.56	0.07	0.38	0.31	0.67	1.11	0.08	0.19	0.24	0.16	0.22
Yb	3.3	1.9	3.6	3.3	2.8	2.1	2.0	3.2	2.3	3.0	2.3
Cr	140	132	43	69	142	520	340	158	61	96	75
Hf	3.5	1.05	2.9	2.5	2.8	3.0	0.97	2.6	3.0	2.3	2.7
V	290	203	510	310	336	300	257	273	146	360	300
Nb	9.7	1.10	6.3	5.5	11.6	19.4	1.24	3.1	2.9	2.3	3.6
Rb	16.4	1.42	12.0	7.8	5.7	0.42	0.3	7.5	48	10.5	34
Ho	1.21	0.64	1.25	1.16	1.04	0.85	0.65	1.03	0.71	1.05	0.80
Cu	107	13.3	25.8	17.2	79	112	174	51	26.4	130	84
Pb	6.5	0.46	0.88	1.49	1.6	0.74	0.27	1.5	2.1	2.1	1.6
Er	3.5	1.8	3.6	3.4	3.0	2.4	2.0	3.0	2.1	2.9	2.2
Ga	17.8	13.7	19.9	16.8	16.6	15.7	11.3	16.8	12.1	16.8	14.6
Cs											
Gd	5.3	2.5	4.9	4.8	4.8	4.5	2.1	3.7	3.5	3.9	4.3

Notes: RD% for major elements is calculated from the standard with the closest true value to the measured sample and are: AGV2 for Al and Ti within ±2%, RGM1 for Na within ±2.4% and remaining elements standard BCR2 as followed Si, Mg and Fe within ±1%, K and Mn within ±2.4%. All values are with according significant figures. Trace elements limits of detection are 0.1ppm, except V, Ni, Zn and Cr which are 1ppm and Cs and Sc at 4ppm. RD% are in the listed order: Y to Pr within 0.8%, Tb to Ni 2.3%, Ce to Lu $\leq$4.1%, Ta to Rb $\leq$6.7% and Ho to Ga $\leq$8.5%.

5 Analytical results

5.1 Petrography

All samples are melanocratic except VP16-23e which is mesocratic. Grain size ranges from phaneritic to very fine to medium grained, except VP16-22c which is aphanitic. Microscopy shows the rocks are dominated by saussuritizised plagioclase (approximately 60% of the mode). Other common minerals present are clinopyroxene, chlorite, rutile and secondary calcite. Rutile shows disequilibrium alteration and pyroxenes are fractured with expansion cracks. The VP16-23 samples shows the least alteration of plagioclase which is slight to moderate. Only sample VP15-10 contains polybaric amphibole with an actinolite core and hornblende rim. VP16-23e has primary quartz. Full mineralogy is presented in the appendix (III). Microscopy reveals VP16-23c to be a volcaniclastic rock composed of angular fragments imbedded in an aphanitic matrix. Therefore, this volcaniclastic sediment cannot be directly compared to the geochemistry from the volcanic rocks and is not plotted in subsequent diagrams. From hand sample observations and microscopy the rocks classify as follows: VP16-23d,a and VP16-22c,b are andesite/basalt; all VP15 samples, VP16-23e, and VP16-22b are gabbro; VP16-23c is volcaniclastic. The rocks are of low metamorphic grade, greenschist to prehnite-pumpellyite facies

5.2 Major elements

Volatile content from loss on ignition (LOI) is within 4 wt% and slightly higher for samples VP16-22b, VP16-23d and VP16-23e with 5.81 wt%, 4.76 wt% and 6.83 wt% respectively. Mobility of sodium and potassium was evaluated by plotting these elements against LOI (Fig. 2). The positive relationship with LOIs suggests potential sodic metasomatism. Samples VP16-23d,e and VP16-22b seem to be most affected. Potassium alteration is only distinguished in VP16-23e and VP16-22b, with the remaining samples forming a cluster (except VP16-23c). Since K and Na alteration could imply metasomatism for mobile trace elements, care is taken when interpreting these oxides. Using le Maitre's (1989) classification scheme (Fig. 3a) the samples are basalts, with the exception of sample VP16-23c (a trachyte) and VP16-23e (basaltic trachyandesite). When samples plot on the dividing line in the classification scheme, the classification for the lower Na value was selected due to the evidence for potassic metasomatism. In the same diagram, the alkalinity of the samples is determined using the subdivisions of Irvine and Baragar (1971). Sample VP16-22b seems to be alkaline, while the remaining samples are sub-alkaline. However, as Na metasomatism is likely associated with sample VP16-22b, it is included in the subalkaline field. Further classification using Miyashiro's (1974) dividing lines indicates that all samples are tholeiitic, with the exception of the calc-alkaline volcaniclastic sample (VP16-23c) (Fig. 3b). The data is compared with Box and Patton (1989) in figure 4; classifications are made with the same reference frames as reported in their diagrams.

Eight major elements were measured. SiO_2 ranges from 46-53 wt%, with sample VP16-23c deviating at 63 wt%. Total iron, Fe_2O_3, ranges from 6-14 wt%. The ratio of ferric to ferrous iron was made as per Middlemost, (1989) using the following Fe_2O_3/FeO ratios: 0.2 for basalts and 0.5 for VP16-23c and 0.35 for sample VP16-23e. The conversion was made by deriving the calculation (see appendix IV). Further major and minor elements range as follows: Al_2O_3 15-19%, CaO 3-16%, MgO 3-9% and Na_2O 2-4.6%. K_2O and TiO_2 concentrations are 0.03-2.7% and 0.6-2.5% respectively. Alumina show a positive correlation with silica, while calcium and magnesium show a negative correlation with silica. P_2O_5 is below the limits of detection (LOD) and therefore not reported in the data table. CIPW normative mineralogy shows the rocks are silica undersaturated, with the exception of VP16-23c which is oversaturated and VP16-23e is saturated. Normative mineralogy is dominated by Anorthite, Albite and Diopside (see appendix V for full CIPW mineralogy).

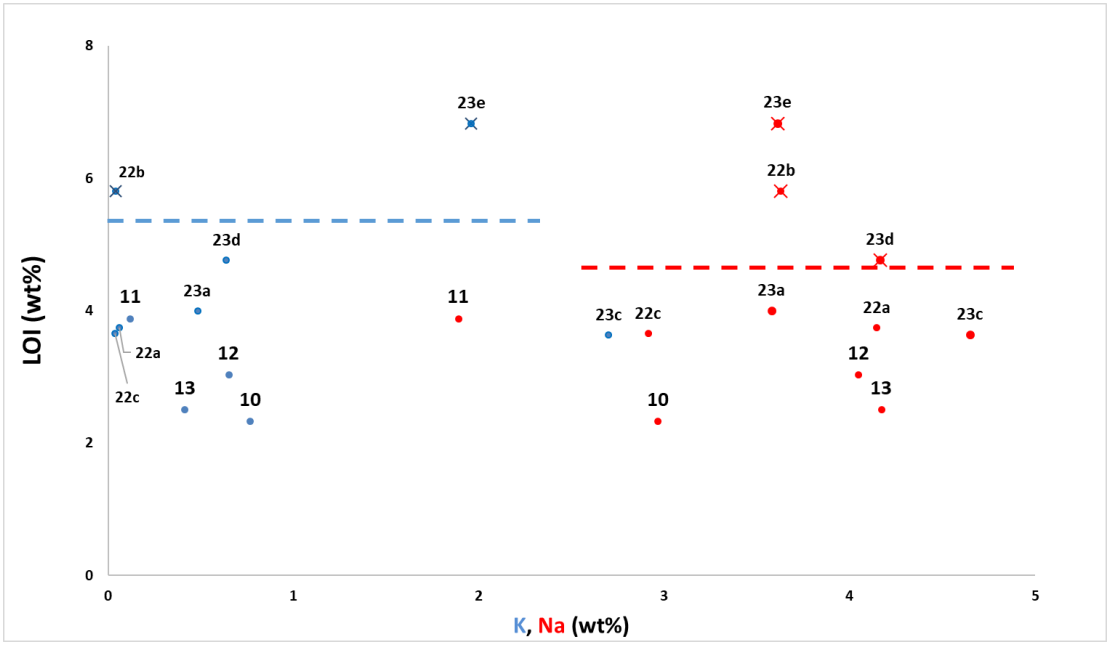

Figure 2. Evaluation of element mobility and metasomatism. LOI plotted against sodium (in red) and potassium (in blue). Dashed line marks limit for LOI and suspected metasomatism. Samples indicating element mobility with high LOIs include VP16-23d, e and VP16-22b for sodium and VP16-23e and VP16-22b potassium

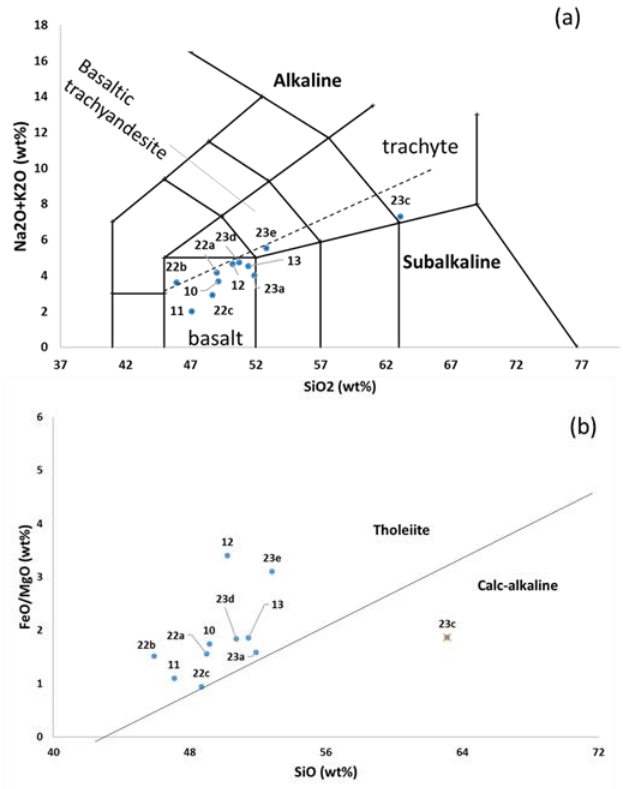

Figure 3. (a) Rock classification (after Le Maitre, 1989) and alkalinity (after Irvine and Baragar, 1971). (b) subalkaline division (after Miyashiro, 1974). The samples classify as tholeiitic basalts, except for VP16-23c (calc-alkaline trachyte) and VP16-23e (tholeiitic basaltic trachyandesite

5.3 Trace elements

A total of 32 trace elements have been analysed (Table 1). Of these Cs is below the LOD and no value is presented. Rare earth elements (REE) and multi-element diagrams (Fig. 4) show element trends normalised to carbonaceous (CI) chondrite values from Sun & McDunough (1989). REE plots (Figs. 4a, b) show light REEs on the left transitioning to heavies to the right. Both REE and multi-element plots (Figs. 4a-d) are organised with increasing incompatibility to the left. All samples are enriched in REE normalised to chondrite. Most samples (Fig. 4a) show a 50-fold enrichment and a near flat trend. $(La/Yb)_N$ range from 0.7 to 2.2. Two samples deviate from this trend: VP15-11 is depleted in light rare earth elements (LREE) relative to the heavy rare earth elements (HREE) and VP16-23e has visibly more pronounced LREE enrichment and $(La/Yb)_N$= 4.2. Outcrop rocks VP16-22a,b show identical behaviour as most of the igneous clasts, while VP16-22c although it displays a similar trend but with a noticeable depletion in LREE to the HREE (Fig. 4b). All samples show a small kink at Eu which continues flat through the HREE.

In the multi-element diagrams (Figs. 4c-d) samples from the outcrop are distinct from the clasts. Enrichment is about 10-times chondrite values but varies from below 10 times up to almost 100-times at the mobile end of the graph. Samples VP15-11 and VP16-22c have lower enrichment levels and slope positively at the most mobile elements.

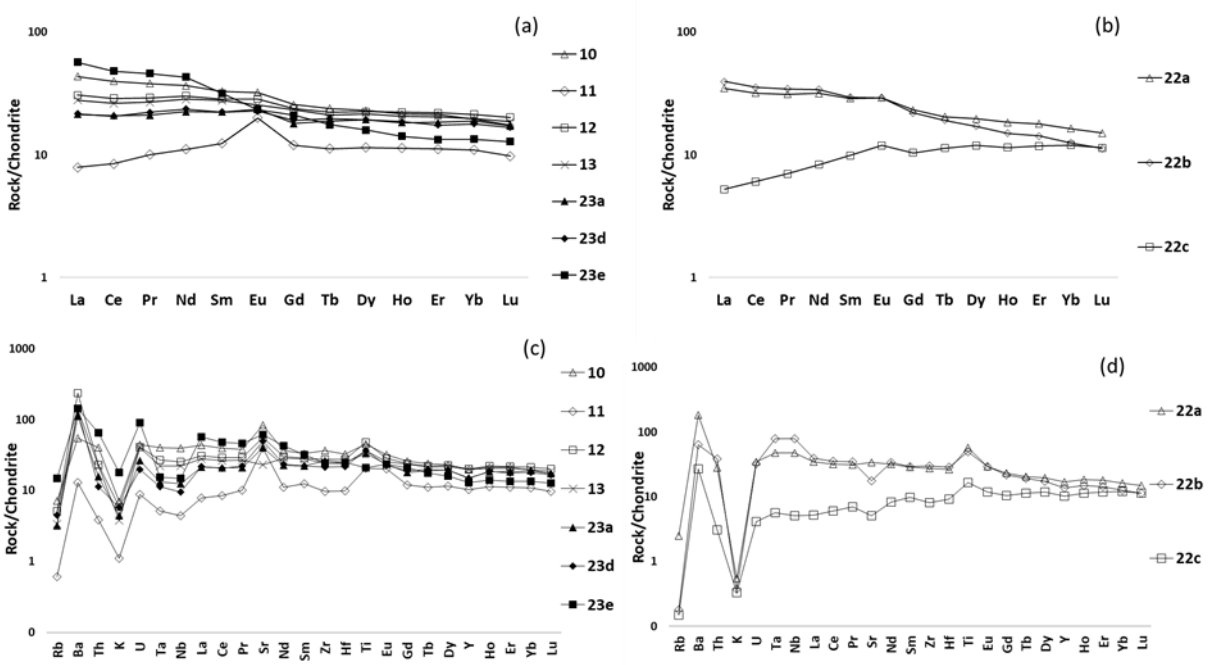

Figure 4. Samples normalised to carbonaceous (CI) chondrite (values from Sun & McDunough, 1989). The trends show great similarity. All samples are enriched relative to CI chondrite. (a, b) Most samples are enriched in LREE relative to HREE, with only samples VP15-11 and VP16-22c showing depletions. (c, d) Multi-element trends stay flat across the most immobile elements and negative anomalies in K and Rb occur. Some sample show Ta and Nb anomalies, while others do not.

All samples are flat through the middle rare earth elements (MREE) and HREE, have a positive inflection at Ti and negative one at K and Rb. Samples VP16-22b,c and VP15-13 show a small drop at Sr while VP16-22a is flat and remaining samples have a positive kink. Samples of VP16-23 show a clear negative Ta-Nb anomaly, whereas in samples of VP15 it is more subdued. In contrast, none of the VP15-22 rocks show Ta-Nb anomalies.

6 Discussion

The core of this study is to determine whether the igneous clasts of the KKB sedimentary deposits have the compositional affinity of arc rocks or if they formed in a continental rift setting. To decrypt the origin of igneous clasts in the Yukon Koyukuk basin sediments, petrographic observations, field relationships and geochemical data (with emphasis on the latter) have been applied. The geochemical data are used to identify geochemical signatures characteristic of specific tectonic settings. This approach allows discrimination between samples of a similar classification (i.e., basalts) from those of different environments (arc versus rift). It also involves a set of assumptions about the samples and their compositions: discrimination diagrams are derived from analyses of samples representing modern tectonic settings and these are used to determine the best fit for older samples. This assumes that the formational mechanisms are the same as in modern environments and that the same chemical signatures were generated in the past. From field relationships and common geochemical features, we also assess the cogeneity of the samples. The final assumption is that the elements used for classifying the rocks represent the original compositions. This means that it is necessary to account for any (metasomatic) alteration that may change the bulk chemistry of the samples.

6.1 Cogenetic melt source

The compilation of evidence points to a comagmatic rock series for the igneous clasts and a separate series for VP16-22 samples.

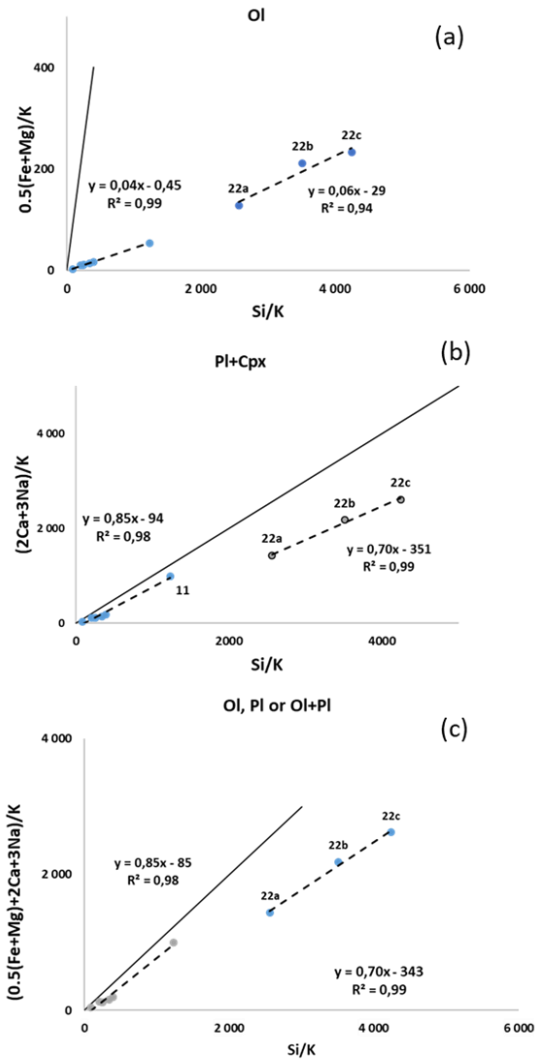

Figure 5. Testing crystal fractionation and the liquid line of descent (LLD). (a) Samples show a strong deviation from the 1:1 Ol line, (b, c) Igneous clasts show good indications for crystallisation of Cpx and Pl. Note the strong deviation in LLD for VP16-22 samples.

Element ratio diagrams can aid determination of the liquid line decent (LLD) (Fig. 5) – this means that a melt generated by crystal fractionation produces linear arrays with strong correlation coefficients (R >0.99 to 0.94). Such linear arrays will define slopes (indicated by solid line in figure 5) of particular values directly correlated with the composition of the mineral phases involved. In figure 5, crystallization of olivine (Ol), clinopyroxene (Cpx) and plagioclase (Pl) are assessed. The crystallization of Pl and Cpx together exert the most control on melt evolution for these basaltic rocks. Samples associated with VP16-22 indicate an

additional mineral is involved along with the crystallisation of Pl and Cpx. Olivine could be involved (given the continuity of slope in figure 5a), but cannot be the sole crystallising mineral phase. Na metasomatism doesn´t seem to disrupt this correlation, which contradicts the observations from figure 2 (alkalis vs LOI) and the Pl alteration seen in thin section. This is most likely due to reduction of the 'metasomatic' effect via combination with the other elements when calculating the ordinate axis. It is possible but unlikely that metasomatism was a closed system. The confidence in the element ratio plots (Fig. 5) is strengthened by the good correlation of the Ol fractionation trend which does not include K or Na; thus alteration is unlikely to have affected these trends. Suspected alterations due to other mechanisms will be discussed later.

In addition, multi-element diagrams reveal very similar trends and values in the HFSE and HREE between the rocks. These uniform values together with the element ratio diagrams indicate that the igneous clasts and outcrop samples are not from the same parent melt, but might be closely related.

6.2 Tectonic setting of KKB igneous clasts

All samples classify as tholeiitic basalts except for the volcaniclastic samples VP16-23c (calc-alkaline trachyte) and VP16-23e (basaltic trachyandesite) (Fig. 3). Tholeiitic basaltic rocks can form in several tectonic environments. To determine if they represent island arc volcanism, the geochemical signature which distinguishes arc basalts from other basalts was assessed. For arc rocks this signature comes from the volatiles and mobile elements which are released from the subducting slab. As the slab descends heat from the mantle drives off volatiles from the hydrous sediment and oceanic crust. These fluid-mobile elements are incorporated into the melt produced above the slab (Best, 2003). Multi-element and tectonic discrimination diagrams can be used to distinguish the tectonic setting for the samples. There are vast numbers of these diagrams but they share a common element: A large number of rocks from different and known environments are analysed and selected elements are plotted against each other. The data points form a cluster and the area they occupy define the outline of the discrimination field. The samples are plotted on diagrams from Kamenetsky et al. (2001), Shervais (1982) and Pearce (1982) (Fig. 6). On all these discrimination diagrams the samples always lie at the arc, OIB and MORB interface. Figure 6a separates the fields of large igneous provinces (LIPs) and peridotites; the KKB samples plot in the OIB towards arc compositional fields. Samples VP16-23e, VP16-22c and VP15-11 have arc compositions. On Shervai's (1982) diagram (Fig. 6b) the samples also trend towards IOB, with some samples extending to MORB. On Pearce's (1982) Cr-Y diagram (Fig. 6c) the samples plot in the island arc field, and again border the MORB field, with samples VP16-22b and VP15-10 just into the MORB field. There is some variation in the classification of the samples between diagrams. Subduction zones produce a vast variety of compositions over the lifespan of the arc and where in the arc melt is formed (Best, 2003). The overall trend in discrimination diagrams is consistently towards Arc/OIB rocks. The multi-element diagrams (Figs. 4c, d) are consistent with this interpretation; they define MORB- to arc-like $(La/Yb)_N$ values of 0.4 to 4.2 indicating a gradational change from LREE depletion relative to HREE to LREE enrichment relative to HREE. This variation in subduction input is interpreted to relate to the release of fluid mobile elements incorporated into the melt. A strong diagnostic island arc signal is a Ta-Nb negative anomaly (Thompson et al. 1984) because these elements remain in amphibole in the subducted residue. Flat MREE and HREE trends are also typical of island arc rocks. VP16-23 samples have the strongest arc signature, which separates them from VP15 clasts that have a less developed Ta- Nb trough. Only VP15-22 samples lack the Ta-Nb trough. From field observations, these

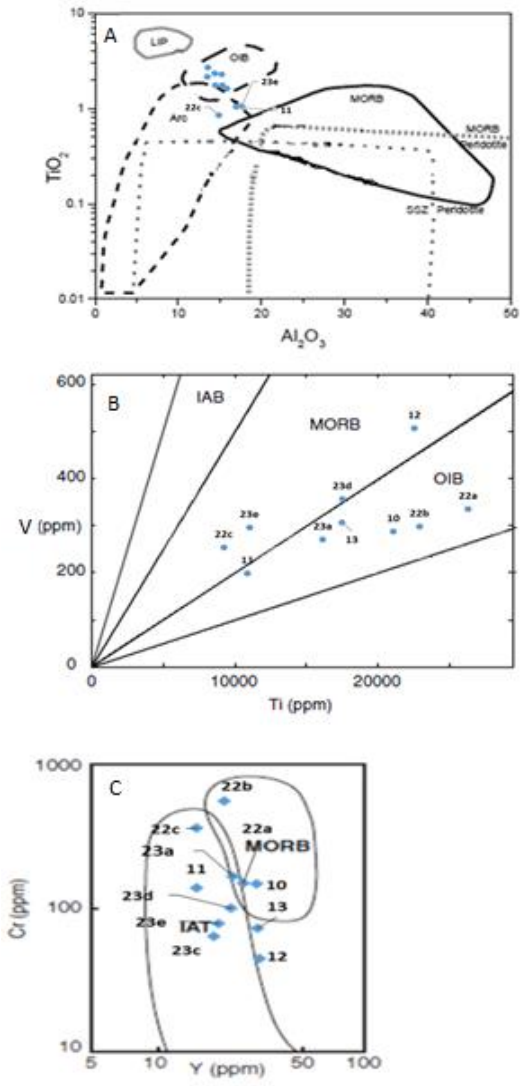

Figure 6. Discrimination diagrams for oceanic basalts (A) TiO2- Al2O3 (after Kamenetsky et al., 2001), (B) V-Ti (after Shervais, 1982) and (C) Cr-Y (after Pearce, 1982).

rocks are pillow basalts (cover photo) and may be related to the Angayucham ophiolite. These observations, combined with their multi-element geochemistry, are consistent with the VP16-22 samples being oceanic basalt of MORB to OIB provenance. The variations seen across the data set is best explained to reflect their relation to and interaction within a juvenile arc or fore-arc setting.

6.3 Relationship to the Koyukuk Terrane

A fundamental part of investigating any sedimentary unit is identifying the source of the deposited material. High terranes bordering a basin are possible source regions. However, it may often be the case that the basins were subsequently fragmented/faulted, or that erosion has stripped away the entire source unit so that it can no longer be found *in situ* and is only represented by clasts in the basin deposits.

Box and Patton (1989) published geochemistry from the volcanic rocks of the KT bordering the KKB to the southwest (Fig. 1). Their work identified four stratigraphic units of Early Mesozoic to Albian age. The data from this study is shown with that from the KT in figure 7. There is a good match with their units 3a, b and c. Box and Patton (1989) describe unit 3 as Lower Cretaceous volcanic rocks with a range of chondrite normalised REE patterns from flat $(La/Yb)_N$= 1 to >15 indicating high LREE enrichment. This study shows less variation in $(La/Yb)_N$ (0.4-2.2) so there is only overlap at the lower concentrations. The basin clasts and unit 3a, b and c show similarities in multi element trends, with flat HREE, HFSE at 10x chondrite, and a Ta-Nb trough. In the preceding paragraph, an arc signature was established. Superimposing the data with those of Box and Patton (1989), their unit 3 plots in the convergent and N-MORB field (Fig. 7a). Analyses from this study represent N-MORB and E-MORB. Rollinson (1993) highlights a possible Ta mobility in altered basalts and this was assessed by plotting Ta vs Y (Fig. 7b) which should be constant as a melt evolves. Indeed, sample VP16-22b remains outside the group while the other samples show a limited spread. Sample VP16-22b together with VP16-22a are the two samples within the B field (Fig. 7a). From the similarity between the KKB data and the KT units 3a, b, and c data of Box and Patton (1989) and the proximity between the KT and the KKB clasts, suggests that the clasts may be derived from the KT. The KT may have been more extensive than seen today, with the KKB clasts representing fragments of the same subduction-arc setting. The KKB clasts define a limited compositional array, whereas

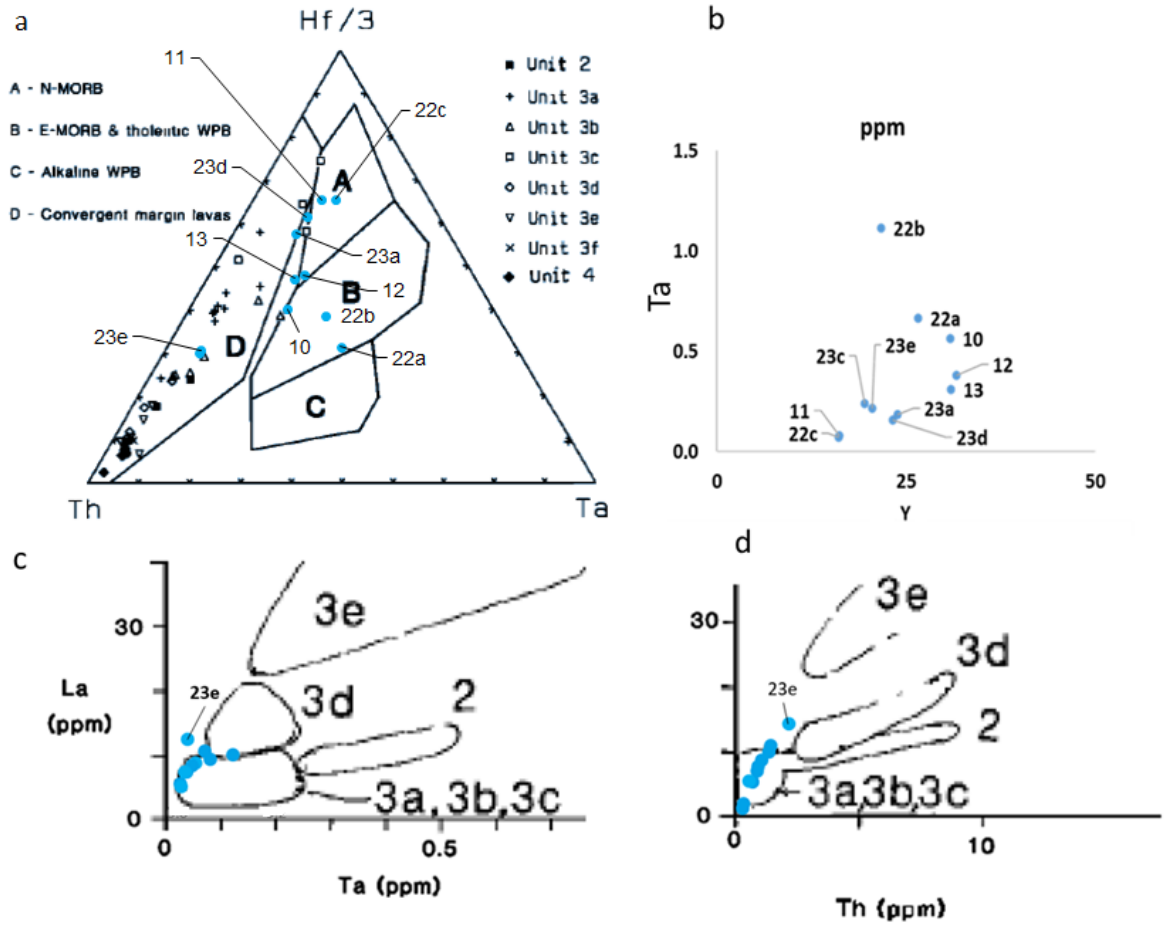

Figure 7. Basalt discrimination diagrams. (a) data from Box and Patton (1989) on diagram of Wood (1980), (b) Ta-Y (ppm) to test mobility of Ta in the samples from this study, (c, d) Box and Patton (1989) data with their units and analyses from this study superimposed (blue).

the KT data (Box and Patton, 1989) shows a much greater diversity. This wide range of compositions can be generated within a single arc (Best, 2003). This is further supported by La/Ta and La/Th ratios of the KKB (Fig. 7c, d). The KKB samples fall within or at the very margin of the same units 3a, b and c of Box and Patton (1998). Future avenues for investigation of the KKB and its clasts could include a comparison of the data from the pillow basalt outcrop (VP15 samples) with published data from the Angayucham Terrane ophiolite; this will help to confirm whether this outcrop is a fragment of the thrusted ophiolite of Angayucham Terrane. Age dating and isotopic data could additionally constrain the source(s) of these clasts.

7 Conclusions

Based on similarities in multi-element data and element ratio diagrams for mineral crystallisation, the data from samples VP15, VP16-22 and VP16-23 are cogenetic. The relationship between these groups is interpreted to derive from a very similar melt source. The rocks formed in different parts of an island-arc system. The textures and trace elements of VP15-22 samples from the outcrop are classified as MORB ophiolite. From the combination of discrimination diagrams and varied strength in arc signature the igneous clasts associated with VP16-23 are interpreted to represent a juvenile arc or forearc; samples from VP15 are IOB (possibly from seamounts) associated with the arc.

These samples correlate well with the KT samples of Box and Patton (1989) (their units 3a, b and c) and supports the interpretation of an arc setting. Differences between our samples and data from Box and Patton (1998) suggest that even if the samples may derive from the same island arc system, they do not represent the exact same unit. Concerns regarding metasomatic alteration is still an issue and some alteration has affected these samples, even if it´s full extent is difficult to determine.

Acknowledgments

To Victoria Pease for guidance and providing an interesting and stimulating project. Dan Zetterberg for instructing on sample preparation. Emelie Axelsson and Curt Broman for analysis.

References

Best M. G. 2003, Igneous and metamorphic petrology 2nd ed, Malden, Blackwell publishing, 283-307

Box S. E. and Patton W. W, 1989, Igneous History of the Koyukuk terrane, western Alaska: Constraint on the origin, evolution and ultimate collision of an accreted island arc terrane. Journal of Geophysical Research 94(B11), 15843-15867

Irvine T. N. and Baragar W. R. A, 1971, A guide to the chemical classification of the common volcanic rocks, Can. J. Earth Science, 8, 523-548

O´Brien T.M., Miller E.L., Pease V., Hayden L. A., Fisher C.M., Hourigan J.K., and Vervoort J.D., in press, Provenance, U-Pb detrital zircon geochronology, Hf isotopic analyses, and Cr-spinel geochemistry of the northeast Yukon Koyukuk Basin, AK: Implication for Alaska interior basin development

Kamenetsy V. S., Crawford A. J. and S. Meffre, 2001, Factors Controlling Chemistry of Magmatic Spinel: an Empirical Study of Associated Olivine, Cr-spinel and Melt Inclusions from Primitive Rocks, J Petrology, 42 (4) 655-671

Le Maitre R. W., Bateman P., Dudek A., Keller J., Lameyre Le Bas M. J., Sabine P. A., Schmid R., Sorensen H., Streckeisen A., Woolley A. R. and Zanettin B., 1989, a classification of igneous rocks and glossary of terms. Blackwell, Oxford

Miyashiro A., 1974, Volcanic rock series in island arcs and active continental margins, American journal of science, 274, 321-355

Morris G and Pease V., Facility document. The Stockholm Petrotectonics X-ray Fluorescence Facility:

Analytical Technique, Parameters, Precision and Accuracy, Petrotectonics Group, Stockholm University

Middlemost E. A. K., 1989, Iron oxidation ratios, norms and the classification of volcanic rocks. Chem. Geol, 77, 19-26

Patton W. W. and Box S. E, 1989, Tectonic setting of the Yukon-Koyukuk Basin and it Borderlands, western Alaska. Journal of Geophysical Research 94(B11) 15807-15820

Pearse J. A., 1982, Trace element characteristics of lavas form destructive plate boundaries, New York, John Wiley & Sons

Rollinson H., 1993, Using geochemical data: evaluation, presentation, interpretation, Routledge, New York, 50-58, 171-199

Shervais J. W., 1982, Ti-V plots and the petrogenesis of modern and ophiolitic lavas, Earth Planet. Sci. Lett., 59, 101-118

S. Sun and McDonough W. F, 1989, Chemical and isotopic systematics of oceanic basalts: implications for mantle composition and processes Geological Society, London, Special Publications, 42, 313-345

Thompson R. N., Morrison, M. A., Hendry G.L. and Parry S. J, 1984, An assessment of the relative roles of crust and mantle in magma genesis: an element approach, Phil. Trans. R. Soc. Lond. A 310, 563-568

Wood D. A., 1980, The application of a Th-Hf-Ta diagram to problems of a tectonomagmatic classification and to establish the nature of crustal contamination of basaltic lavas of the British tertiary volcanic province, Earth Planet. Sci. Lett. 50, 11-30

Winter J. D., 2014, Principles of Igneous and Metamorphic Petrology 2nd ed, London, Pearson Education Limited

Appendix

I Sample Photographs

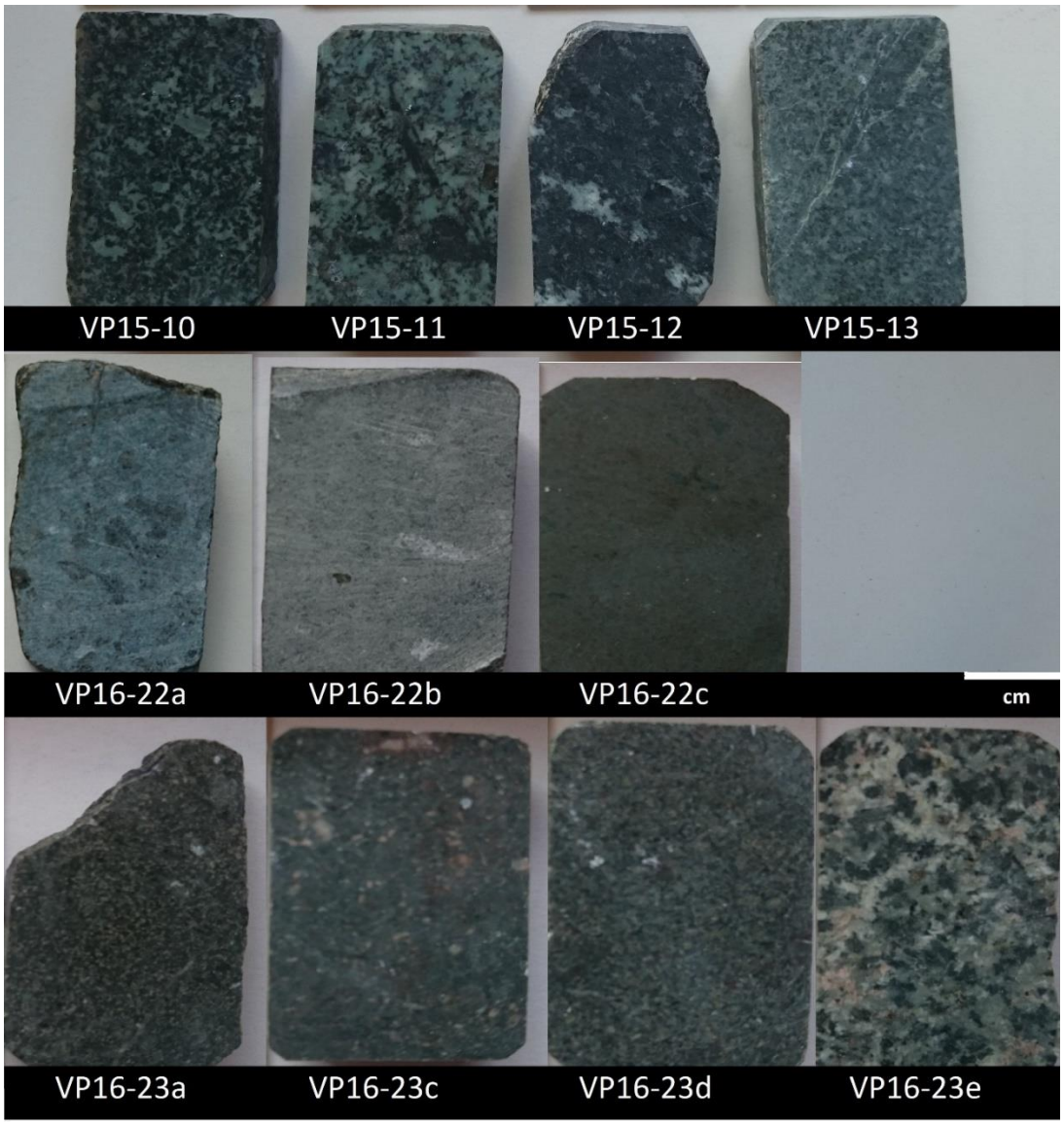

II Methods

Sample preparation

To attain sample homogeneity for XRF and LA-ICP-MS analysis, glass discs are fused from pulverized and dried aliquots. Prior to crushing all weathered surfaces were sawed away and cleaned from saw-metal on a steel grinding disc with abrasive aggregate silicon carbide. Any present contamination particles were removed by an ultra sound bath. Pulverising was done with a vibratory disk mill Retsch RS200 at 1400rpm at times between 120-50s. For LOI 5,0000g ±0,0002 pulverized sample was heated in acid washed ceramic crucibles at $1000^{o}C$ for 3 hours to remove structurally bound volatiles. Glass discs for XRF and LA-ICP-MS analysis were made from 5,0000 g±0,0002g Lithium borate flux ($66\%Li_2B_4O_7$ $+34\%LiBO_2$) and 2,0000g ±0,0002g sample aliquot fused in platinum crucibles with a Phoenix autofuser onto platinum cast. The discs were first used in the XRF analysis and afterwards crushed and fragments mounted in Epoxy and polished to expose a clean sample surface for La-ICP-MS trace element analysis.

XRF

XRF is a non-destructive Wave Dispersive Spectrometry (WDS) used to analyse element composition of a sample. Atoms will fluoresce a spectrum of x-ray energy when bombarded with a high-energy beam. The beam: x-ray or gamma ray excites the inner electrons enough to eject from the hosting atom, higher level electrons rearrange themselves to fill the gap and while doing so fluoresce an energy equal to the difference in energy between the ejected and high level electron. This emitted energy is much lower than the initial beam from the XRF. Each element will have a unique and specific emission spectrum which can be detected, measured and used to identify element composition in a sample. The intensity of the emitted energy is proportional to the concentration. This is measured in counts per second and together with a calibration allow a quantitative measure of the concentration of each element. The XRF uses Compton scattering or inelastic scattering where energy is transferred, however there is always background noise of the matrix in the form of Rayleigh scattering/elastic scattering where energy is preserved this and other factors such as re-detection of dispersed energy influence the resolution of the instrument and affect the detection limits and error margins. These are minimised and determined by calibrating the instrument before analysis. This was done on international standards AVG-2, BCR-2 and RGM-1 as known and unknown standards. The quality of the calibration is good with 95% certainty 2σ within 0.02. The Rigaku ZSX Primus II at Stockholm University is equipped with a thin Beryllium window, Rhenium X-ray tube (Morris and Pease, facility document).

LA-ICP-MS

The Epoxy mounted samples are shot with a laser, dispersing a small cloud of sample. Helium and argon carrier gas is used to transport the sample particles into the ICP chamber. In the ICP a high temperature torch ionizes the sample aerosols. The ionized particles are focused further towards the detector passing quadrupole rods. The rods create magnetic field which causes the ions to wobble as they pass slowing them down. Each element will wobble to a different degree and the delay is characteristic to each element and used to identify the composition of the sample. The detector will then register the hits as counts per second which is proportional to the concentration of the element in the sample. Calibration is made with internal standard NIST-612 and secondary unknowns BCR-2 and SARM-1. 5 analyses per sample were made set at 20 seconds background, 40 seconds laser-on, 10 seconds wash-out. Analytical conditions were as followed; laser energy intensity 7.3 J/cm^2, spot size 150μm, laser pulse frequency 10 Hz.

III Petrography

VP15-10

Mineralogy

Pl, Chl, Rt, Prh, Act, Hbl, Ep

Textures

Interlocking grains, equigranular, Heavy saussuritization of Pl and disequilibrium Rt, polybaric amphibole; Hbl core Act rim

VP15-11

Mineralogy

Pl, Cpx, Chl, Prh, Rt, Ser, Srp, Zeo

Textures

Interlocking grains, Heavy saussuritization of Pl, serpentinisation, fracturing in CPX, some zeolite filling vesicles

VP15-12

Mineralogy

Pl, Cpx, Rt, Ep, Ser, Cal, Srp

Textures

Moderate to heavy saussuritization of Pl, trachytic texture, expansion cracks in Cpx, volcanic

VP15-13

Mineralogy

Pl, Px, Ser, Prh, Rt, Cal, Srp

Textures

Heavy saussuritization of Pl, volcanic

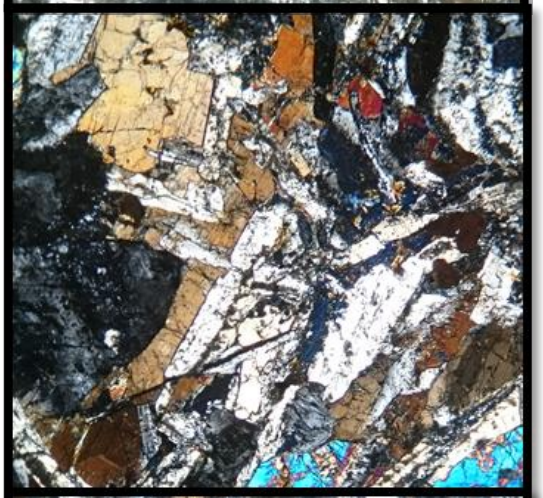

VP16-22a

Mineralogy

Ksp, Cpx, Cal, Rt

Textures

Slight alteration, come calcite aggregates,
Px with expansion cracks, some devitrified glass

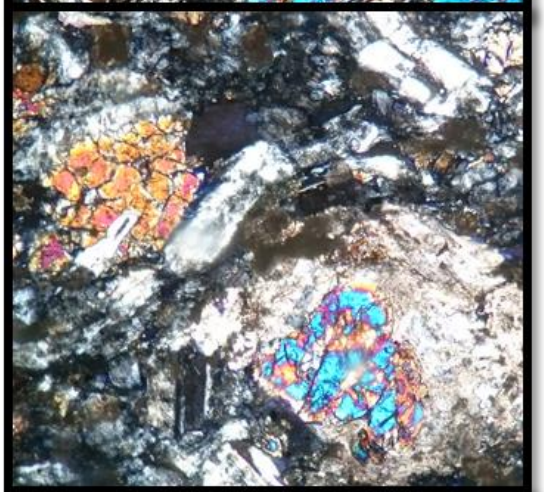

VP16-22b

Mineralogy

Pl, Px, Chl, Cal

Textures

Moderare Pl alteration, glomeroporphyritic calcite filling vesicles

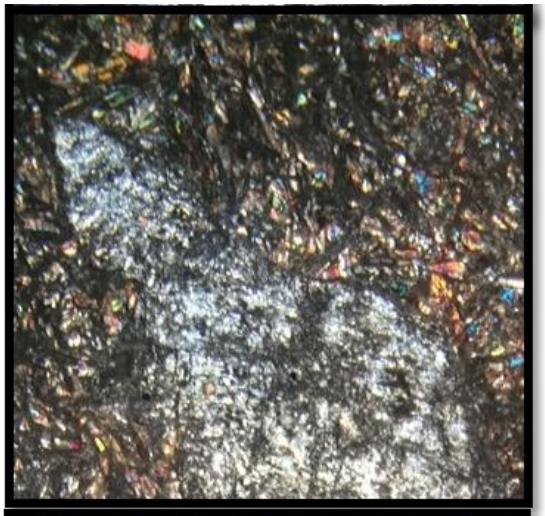

P16-22c

Mineralogy

Pl and mafics

Textures

Aphanitic, volcanic, heavy alteration

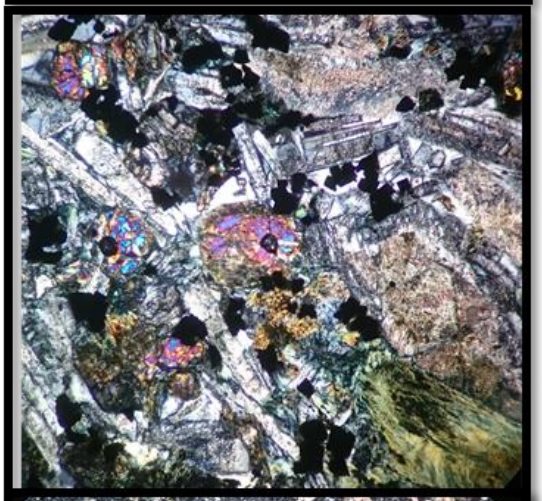

VP16-23a

Mineralogy

Ksp, Pl, Cpx, Chl, Cal, opaques

Textures

Interlocking grains, secondary calcite vein, slight to moderate alteration, some devitrified glass

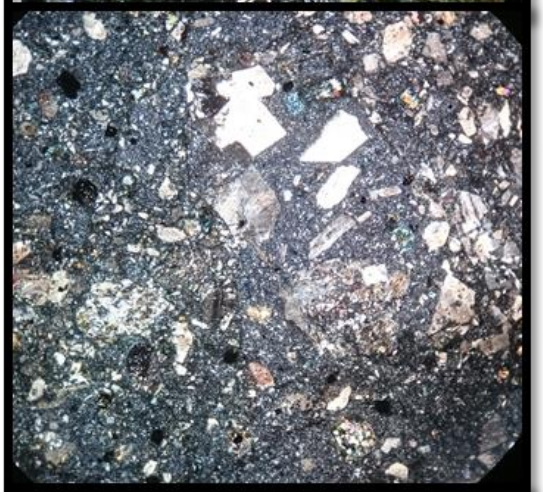

VP16-23c

Mineralogy

Ksp, Qtz, Chl, Cal

Textures

Volcaniclastic, aphanitic matrix

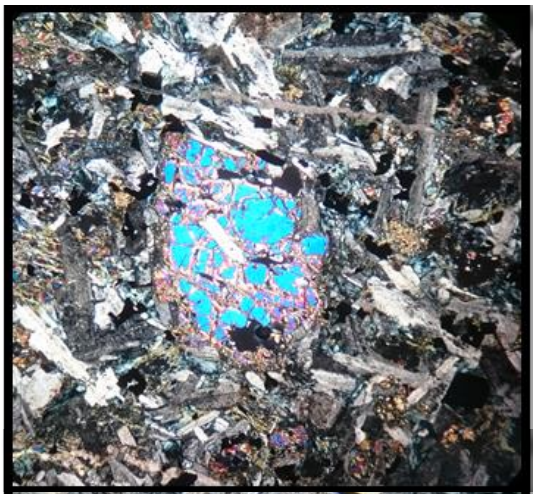

VP16-23d

Mineralogy

Ksp, Chl, Cpx, Cal, Zeo

Textures

Volcanic, possibly devitrified glass present, zeolite filled vesicles, moderately altered

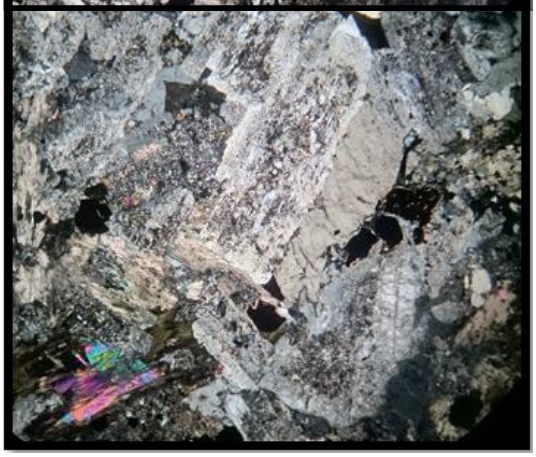

VP16-23e

Mineralogy

Ser, Ksp, Pl, Qtz, Chl, Prh

Textures

Moderate alteration and saussuritization of Pl, only sample with primary Qtz

IV Ferric Ferrous Iron conversion with Middlemost ratio

R→ Middlemost ratio for rock type classified by Le Maitre (1989)

Fe_xO_y → wt%

Fe_xO_yt → total iron as specified oxide

FeO= 71.844M

Fe_2O_3=159.69M

$2*FeO \not\rightarrow Fe_2O_3$

$\frac{2*FeO}{Fe_2O_3}=\frac{143.688}{159.69}=0.8998$

$FeO = Fe_2O_3 * 0.899$

$Fe_2O_3t = Fe_2O_3 + FeO/0.8998$

$Fe_2O_3 \div FeO = R$

$Fe_2O_3t = (FeO*R) + FeO/0.8998$

$Fe_2O_3t = FeO * (R + 1/0.8998)$

$FeO = Fe_2O_3t \div (R + 1/0.8998)$

$Fe_2O_3t = Fe_2O_3 + FeO/0.8998$

$Fe_2O_3t = Fe_2O_3 + ((Fe_2O_3/R) / 0.8998)$

$Fe_2O_3t = Fe_2O_3 * (1+ (1/R *0.8998))$

$Fe_2O_3 = Fe_2O_3t/1+(1/(R*0.8998)$

$Fe_2O_3 = (Fe_2O_3t*R*0.8998) \div (R*0.8998+1)$

V CIPW Normative mineralogy

sample	VP15-10	VP15-11	VP15-12	VP15-13	VP16-22a	VP16-22b	VP16-22c	VP16-23a	VP16-23c	VP16-23d	VP16-23e
mineral	CIPW normative mineralogy wt%										
Qtz									12.7		0.5
An	25.3	41.3	25.6	23.6	22.3	26.9	31.4	21.3	15.0	25.2	30.0
Ab	25.1	11.3	34.3	35.3	32.6	21.2	23.5	34.1	39.4	35.2	30.5
Or	4.5	0.7	3.9	2.4	0.4	0.2	0.2	0.35	16.0	3.8	11.6
Ne		2.6			1.4	5.1	0.6	1.38			
Di	24.5	32.6	12.6	15.9	22.2	21.9	23.1	22.17		9.5	11.5
Hyp	4.1		10.2	9.1					12.7	8.7	10.3
Ol	9.6	7.9	6.0	7.7	13.5	17.1	17.5	13.44		11.5	
Ill	3.8	1.8	4.1	3.1	4.9	4.2	1.4	4.88	1.2	3.1	1.8
Mt	2.8	1.9	3.2	2.7	2.7	3.0	2.2	2.71	2.9	2.8	3.4
Ap	0.3	0.1	0.2	0.2	0.3	0.3		0.25	0.3	0.2	0.5

CIPW is calculated on normalised values following steps of Winter J.D. (2014)